Research in Astronomy and Astrophysics, 24:015011 (14pp), 2024 January https://doi.org/10.1088/1674-4527/ad0428

On the Identification of N-rich Metal-poor Field Stars with Future Chinese Space Station Telescope

Jiajun Zhang[1,2], Baitian Tang[1,2], Jiang Chang[3], Xiangxiang Xue[4], José G. Fernández-Trincado[5], Chengyuan Li[1,2], Long Wang[1,2], Hao Tian[6], and Yang Huang[7,4]

[1] School of Physics and Astronomy, Sun Yat-sen University, Zhuhai 519082, China; tangbt@mail.sysu.edu.cn
[2] CSST Science Center for the Guangdong-Hong Kong-Macau Greater Bay Area, Sun Yat-sen University, Zhuhai 519082, China
[3] Purple Mountain Observatory, Chinese Academy of Sciences, Nanjing 210034, China
[4] Key Lab of Optical Astronomy, National Astronomical Observatories, Chinese Academy of Sciences, Beijing 100101, China
[5] Instituto de Astronomía, Universidad Católica del Norte, Av. Angamos 0610, Antofagasta, Chile
[6] Key Lab of Space Astronomy and Technology, National Astronomical Observatories, Chinese Academy of Sciences, Beijing 100101, China
[7] School of Astronomy and Space Science, University of Chinese Academy of Sciences, Beijing 100049, China
Received 2023 July 9; revised 2023 September 29; accepted 2023 October 10; published 2023 December 18

Abstract

During the long term evolution of globular clusters (GCs), some member stars are lost to the field. The recently found nitrogen-rich (N-rich) metal-poor field stars are promising candidates of these GC escapees, since N enhancement is the fingerprint of chemically enhanced populations in GCs. In this work, we discuss the possibility of identifying N-rich metal-poor field stars with the upcoming Chinese Space Station Telescope (CSST). We focus on the main survey camera with *NUV, u, g, r, i, z, y* filters and slitless spectrograph with a resolution about 200. The combination of *UV* sensitive equipment and prominent N-related molecular lines in the *UV* band bodes well for the identification: the color–color diagram of $(u-g)$ versus $(g-r)$ is capable of separating N-rich field stars from normal halo stars, if metallicity can be estimated without using the information on *u*-band photometry. Besides, the synthetic spectra show that a signal-to-noise ratio of 10 is sufficient to identify N-rich field stars. In the near future, a large sample of N-rich field stars found by CSST, combined with state-of-the-art *N*-body simulations will be crucial to deciphering GC-Galaxy co-evolution.

Key words: stars: chemically peculiar – stars: abundances – techniques: photometric – techniques: spectroscopic

1. Introduction

According to most recent surveys of globular clusters (GCs), almost all exhibit the phenomenon of multiple stellar populations (MPs, Gratton et al. 2012; Schiavon et al. 2017a; Masseron et al. 2019; Nataf et al. 2019; Mészáros et al. 2020). A feature of MPs is chemical inhomogeneity of member stars, which is shown via an anti-correlation between nitrogen (N) and carbon (C), or an anti-correlation between sodium (Na) and oxygen (O), or an anti-correlation between aluminum (Al) and magnesium (Mg). The community usually considers this as a consequence of different levels of enhancement of the primordial population, and the "first generation" (FG) and "second generation" (SG) are referred to as primordial and enriched populations, respectively. Typical SG stars exhibit a different chemical abundance pattern than normal field stars in a given metallicity, with enhanced N, Na, (sometimes helium (He), Al and silicon (Si)), but depleted C and O (and sometimes Mg).

The unique chemical fingerprint of SG stars is particularly suitable for tracing the evolution of individual stars formed in GCs. Due to the dynamical evolution of stars in GCs (including two-body relaxation and ejection) and their tidal interaction with the Milky Way (MW), GC stars are lost to the field (e.g., Weatherford et al. 2023). Identifying these GC escapees in the field is crucial to evaluating different stellar escape mechanisms and estimating their contribution to the MW halo. These GC escapees may not maintain their dynamical properties for long, but chemistry can be preserved along their life time. Though FG stars are almost chemically identical to halo field stars, SG stars show clear distinguishable chemical features. Among the chemical peculiarity of various light elements that we mentioned before, N enrichment is the most economic one to be identified, thanks to the CN molecular lines. These molecular features can be easily found in large spectroscopy surveys, even with a spectral resolution down to ~ 1800. Using the low-resolution optical spectra from the SEGUE survey (Yanny et al. 2009) and high-resolution near-infrared spectra from the APOGEE survey (Majewski et al. 2017), a large number of N-rich field stars have been found in the MW and its satellite galaxies (e.g., Martell & Grebel 2010; Martell et al. 2011, 2016; Schiavon et al. 2017b; Fernández-Trincado et al. 2020, 2021). In addition, the LAMOST survey (Zhao et al. 2012) with the largest number of stellar spectra available joins the quest: Tang et al. (2019, 2020) found ~ 100 N-rich metal-

poor field stars, which were later proved to be chemically identical to GC member stars (Yu et al. 2021).

However, a much larger sample of N-rich field stars is required to fully evaluate their escaping mechanism and the contribution of GC escapees to the MW halo. In that sense, photometric surveys or spectroscopic surveys with lower spectral resolution could be more efficient in searching for N-rich field stars. In the near future, the upcoming Chinese Space Station Telescope (CSST) will greatly increase the sample size of N-rich field stars. Its capability to obtain ultraviolet images and spectra makes it straightforward to detect N-enrichment, due to the NH and CN molecular bands in this wavelength range (300–450 nm). The CSST is scheduled to be launched around 2024 and will share the same orbit with the Chinese space station. Its main survey module has a large field of view (1.1 square degree) and a high spatial resolution ($\sim 0\farcs15$). The limiting magnitudes in the *u* and *g* bands are expected to be 25.4 mag and 26.3 mag (AB magnitude) respectively for point sources (Zhan 2021). The main survey module will obtain multi-band imaging data (*NUV* and *ugrizy*) and slitless spectra ($R \sim 200$, Zhan 2021) in 17,500 square degrees of the sky in its planned ten-year observation. There are also four affiliated instruments on board CSST: Multi-channel Imager (MCI), Integral Field Spectrograph (IFS), Cool Planet Imaging Coronagraph (CPIC) and Terahertz Receiver (THz). Li et al. (2022) demonstrated the possibility to disentangle stellar populations with different abundances of He, C, N, O and Mg with MCI/CSST photometry. In this work, we will estimate the capability of identifying N-rich field stars with photometry and slitless spectra from the main survey camera.

This paper is organized as follows. Section 2 introduces the methodology of generating a mock photometric catalog for MW halo stars, where N-rich field stars are considered. Next, we estimate the feasibility of separating N-rich field stars from normal halo stars with the color–color diagram (CSST main survey camera filters) and slitless spectra (Section 3). Section 4 and Section 5 are devoted to discussions and conclusions, respectively.

2. Method

The logic behind identifying N-rich stars[8] with *UV*-related photometry and spectra is their strong NH and CN features in this wavelength range (Figure 1). The *u*-band filter in the CSST main survey camera covers NH3400 and CN3839 molecular lines, while the *g*-band filter covers CN4142 and CH4300 molecular lines. The different profiles of molecular lines caused by peculiar C and N abundances may render a noticeable change in *u*-band or *g*-band magnitudes.

In order to estimate the possibility of identifying N-rich stars under a situation as realistic as possible, this work uses the smooth halo catalog[9] from the CSST Mock Catalog of Stellar Halo (J. Chang et al. 2023, in preparation). The GALAXIA software (Sharma et al. 2011), which is based on the *N*-body simulation from Bullock & Boylan-Kolchin (2017), is used to generate a stellar halo of the MW. The stellar halo catalog includes six-dimensional kinematic parameters (positions and velocities), as well as information such as mass, age, metallicity, effective temperature and luminosity for each star. Considering the footprint of CSST, the stellar halo catalog only includes stars with a galactic latitude of 25° or higher. GALEVNB (Pang et al. 2016) is used to generate the CSST photometric magnitudes based on these stellar parameters by convolving theoretical spectra with the CSST main camera filters.[10] So, this catalog also includes the photometric magnitudes in the CSST main camera filters.

In the previous catalog, we assume a solar abundance pattern with $[C/Fe] = 0$ and $[N/Fe] = 0$ for all stars. In reality, however, non-solar chemical abundances (e.g., C and N) can change the depth of feature lines in the spectra, which affects the corresponding photometric magnitudes. To obtain the magnitude differences between non-solar and solar chemical patterns, we generate the corresponding synthetic spectra ($R \sim 200$) and convolve them with the CSST main camera filters. The publicly available tool, ISPEC (Blanco-Cuaresma et al. 2014; Blanco-Cuaresma 2019), is employed to generate synthetic spectra, where we use the radiative transfer code and line lists from SPECTRUM (Gray 1999), MARCS model atmospheres (Gustafsson et al. 2008) and Asplund et al. (2009) solar abundances. Finally, we add these magnitude differences to photometric magnitudes from the aforementioned catalog, and we obtain a new catalog that considers a non-solar chemical pattern.

3. Results

3.1. Photometric Identification of N-rich Giant Stars

Since C and N abundances for giant stars may substantially change after they go through first dredge-up and extra-mixing, we separate the giants and dwarfs in the following photometric identification of N-rich stars. Giant stars with $\log g < 3.0$ were selected, while blue horizontal branch (BHBs) stars on the Kiel diagram were discarded, since high temperature would destroy C and N related molecules. Figure 2 shows the Kiel diagram and the color indicates the number density of sample stars. Following the selection criteria and statistical results presented in Tang et al. (2020), (1) we limited the metallicity range of our sample stars to $-1.8 < [Fe/H] < -1.0$, and (2) we assumed that 1% of the sample stars are N-rich stars and 99% are normal stars.

In order to simulate stars with real C and N abundances, we set the chemical patterns of N-rich giants and normal giants as follows: (1) normal giants. We used red giant stars from

[8] Since "field" only indicates a star is not located inside any star cluster, dropping it would not affect any other ongoing project.

[9] Background halo stars.

[10] http://svo2.cab.inta-csic.es/svo/theory/fps3/

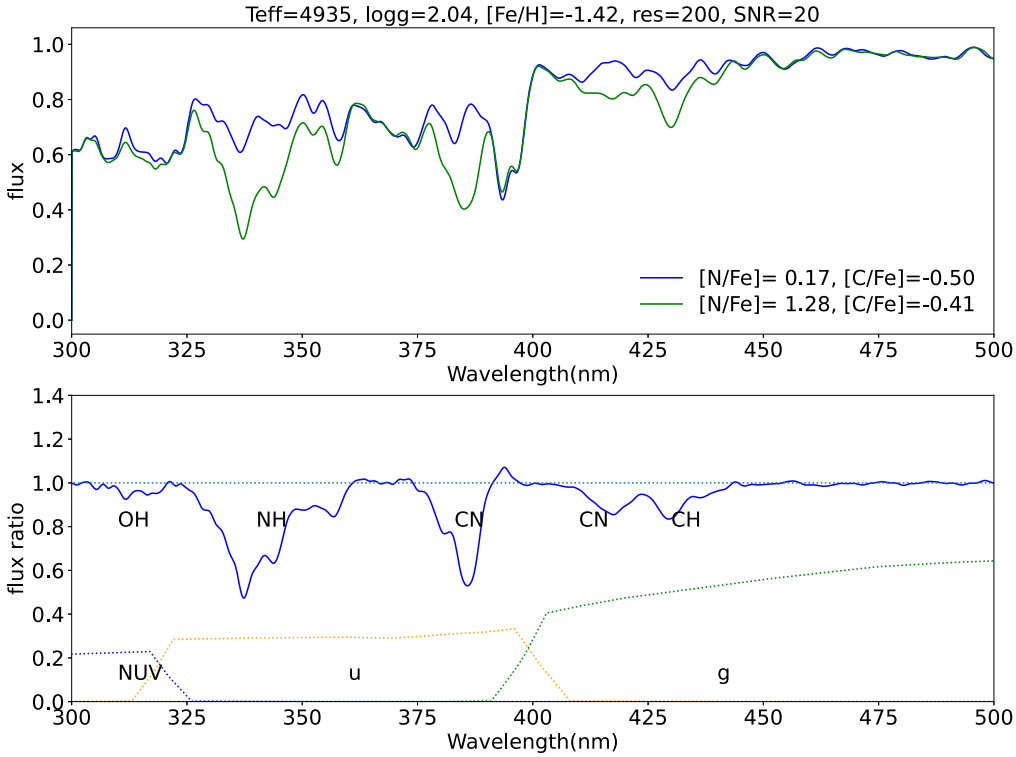

Figure 1. The spectral comparison between two stars with different N enrichment. The upper panel shows two spectra of an N-rich giant star (green line) and a normal giant star (blue line). They have the same atmospheric parameters ($T_{\rm eff}$, $\log g$ and [Fe/H]) but different C and N abundances. The atmospheric parameters, spectral resolution and SNR are displayed in the figure title. The C and N abundances are listed in the bottom-right. The lower panel displays the flux ratio between the two spectra. The locations of OH3200, NH3400, CN3839, CN4142 and CH4300 are labeled. The horizontal dashed line represents a flux ratio of 1.0. The transmission curves of three CSST filters (*NUV*, *u* and *g*) are represented by dashed lines with different colors in the bottom.

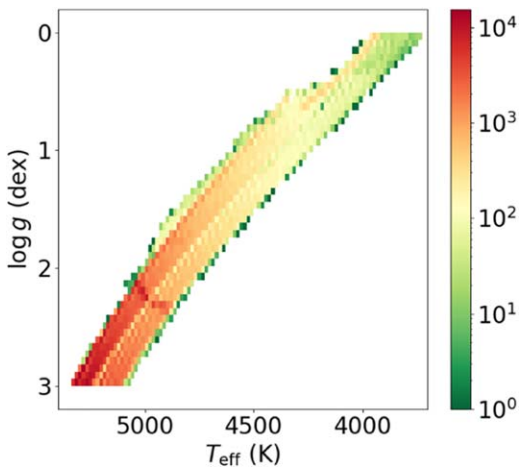

Figure 2. The Kiel diagram of the selected giant stars, with color representing the number density.

Shetrone et al. (2019) as reference and fitted the correlations between C(N) abundances and surface gravity (Figure 3), since C and N abundances would change as a star climbs up the red giant branch (RGB). For a star with given surface gravity, we first estimated the expected values of C and N from the fitted correlations, and then added a random error which follows a Gaussian distribution with $\mu = 0$ dex, $\sigma = 0.2$ dex. (2) N-rich giants. The C abundance of N-rich (field) giants is yet debated, and here we follow the distribution of normal giants. While for their N abundance, we follow the observational results of B. Tang et al. (2023 in preparation), where we set the expected value to be 1.2 dex, and its error also follows a Gaussian distribution with $\mu = 0$ dex, $\sigma = 0.2$ dex. We then generate new photometric magnitudes according to Section 2.

After exploring the color–magnitude diagram and color–color diagram of different combinations of CSST filters, we found that $u - g$ versus $g - r$ is a potential diagnostic color–color diagram to separate stars with different N enrichment, since we have shown that *UV* and blue filters are particularly sensitive to N enrichment in Figure 1. In order to identify more N-rich stars, we divided the metallicity range ([−1.8, −1.0]) into four different bins with equal bin size. Figure 4 displays the results in the metallicity bin of [−1.2, −1.0].[11] We rebinned the normal giant stars on $g - r$ with a bin width of 0.04 mag

[11] The color–color diagrams at other metallicity ranges can be found in Figure A1 in Appendix.

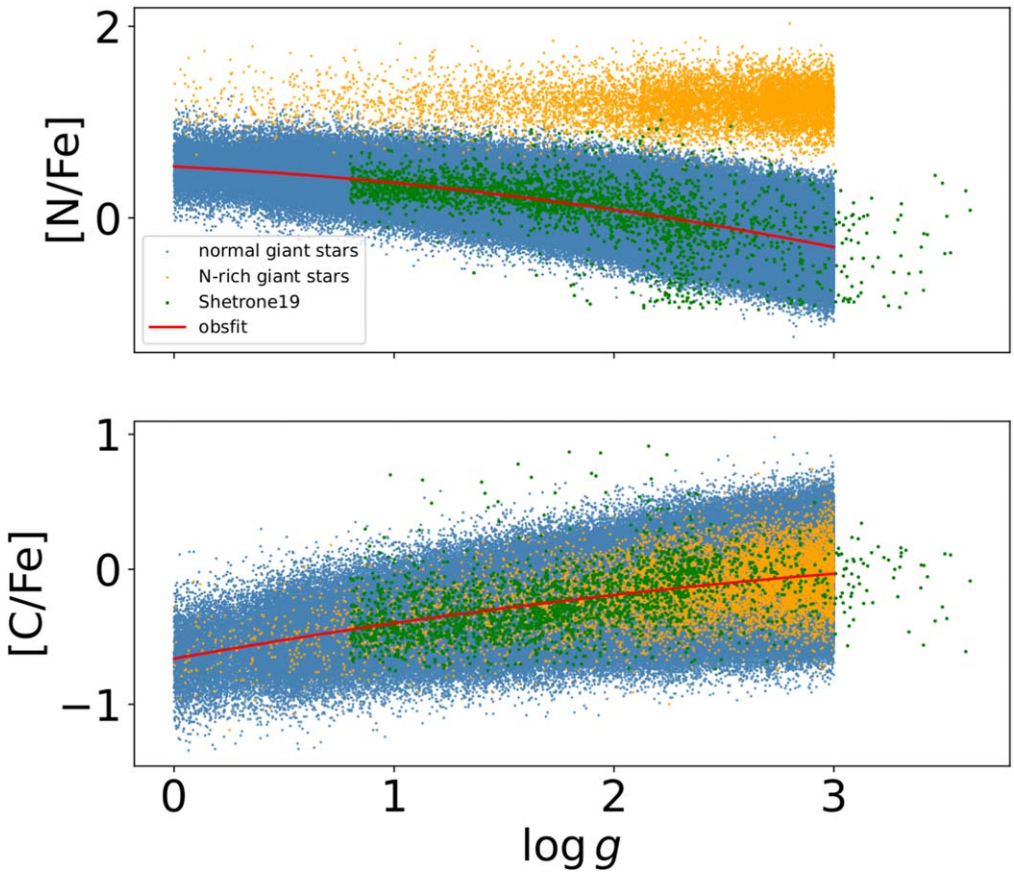

Figure 3. The abundances of C and N for N-rich (orange dots) and normal giant stars (blue dots) as a function of $\log g$. Green dots represent red giant stars from Shetrone et al. (2019), and red lines are relationships between N(C) abundances and surface gravity for the Shetrone sample. See the text for more details.

and calculated their 100% quantile in $u-g$[12] for each bin. After obtaining the 100% quantile points for all the $g-r$ bins (red points in Figure 4), we fitted a fifth-order polynomial to these quantile points (red curve in Figure 4). The coefficients of the polynomial are listed in Table 1. Stars on the left-hand side of the red curve should be a sample of pure N-rich giant stars. However, the real situation is slightly more complicated: the pollution rate (Table 1) is not zero, because (1) we binned $g-r$ with a step size of 0.04; (2) the red curve (polynomial fit) may not follow exactly the red points. We also calculated the hit probability (Table 1), which is defined as the ratio of identified N-rich stars (on the left of the red curve) to all N-rich stars. According to Table 1, the hit probabilities are large for all metallicity bins including the full metallicity bin ([−1.8, −1.0]), suggesting the color–color diagram of $u-g$ versus $g-r$ is a potential way to separate N-rich stars from normal stars. By comparing the hit probabilities at different metallicity ranges, we find that the bins with higher metallicity ([−1.2, −1.0] and [−1.4, −1.2]) show larger values, because of stronger molecular features at higher metallicity. The hit probabilities at divided metallicity ranges are larger than that at the full metallicity range, suggesting that subdividing the metallicity range can help us select more N-rich giant stars.

[12] The maximum $u-g$ value for a normal giant star sample.

3.2. Photometric Identification of N-rich Dwarf Stars

Due to the vast number of dwarf stars in our catalog, we randomly drew 1% out of the dwarf star sample ($\log g > 4.0$, $-1.8 < [\mathrm{Fe/H}] < -1.0$) to save computational time. Given that the capability of identifying N-rich stars would not be affected by the sample size after it reaches a statistically significant number, we consider our simplified dwarf star sample ($\sim 10^6$) sufficient for the following discussion. The Kiel diagram (Figure 5) shows that our sample covers the expected $T_{\rm eff}$ and $\log g$ parameter space. For N-rich dwarf stars (1% of our simplified dwarf star sample), their [N/Fe] values are set as the expected value of 0.8 dex plus a random error which follows a Gaussian distribution with $\mu = 0$ dex, $\sigma = 0.2$ dex, and their [C/Fe] values are set as the expected value of −0.26 dex plus a random error which follows a Gaussian distribution with $\mu =$ 0 dex, $\sigma = 0.2$ dex. Then, we calculated their new photometric

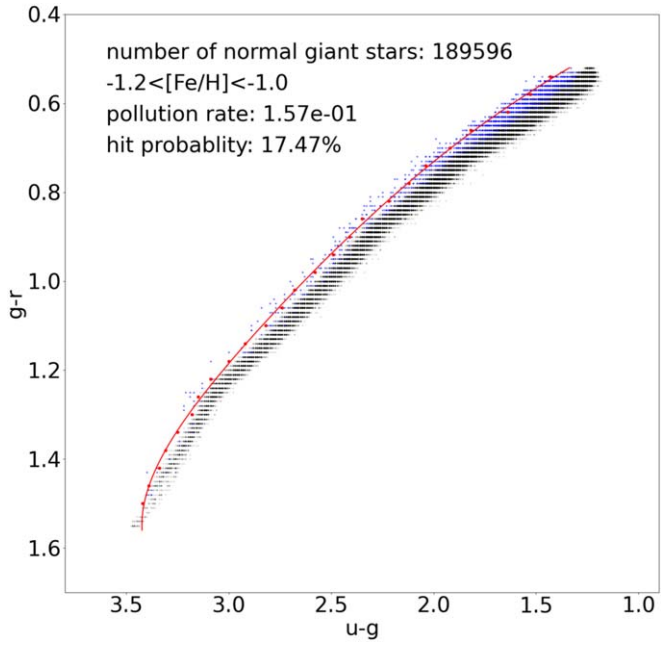

Figure 4. $u-g$ vs. $g-r$ for N-rich giant stars (blue) and normal giant stars (black) at $-1.2 < [\mathrm{Fe/H}] < -1.0$. We rebinned the normal giant stars on $g-r$ with a bin width of 0.04 mag. We calculated the 100% quantile in $u-g$ for each bin. A fifth-order polynomial fit was fitted to these quantile points (red points) and the red curve is the corresponding curve of the polynomial fit. We labeled the number of normal stars, the metallicity range, the pollution rate, and hit probability in the upper-left.

magnitudes according to Section 2. Since normal dwarf stars (the other 99%) are usually not chemically enhanced, solar chemical pattern is assumed, and no changes were made to their photometric magnitudes.

Figure 6 shows the $u-g$ versus $g-r$ color–color diagram of N-rich dwarf stars and normal dwarf stars at the metallicity bin of $[-1.2, -1.0]$.[13] Following a similar procedure as for the giant stars, we obtained the border between two populations (red curve) in Figure 6. However, this border was obtained only between the $g-r = 0.28$–1.40 mag (same for all the metallicity bins), because (1) the two populations have significant overlap at $g-r < 0.28$ mag, and it is difficult to separate them, and (2) the fitting is significantly worse if it is extended to $g-r > 1.40$ mag, which corresponds to the less constrained "knee" feature in the lower main sequence. We show the pollution rate, hit probability and coefficients of division lines at different metallicity ranges in Table 2. According to Table 2, for all metallicity bins including the full metallicity bin ($[-1.8, -1.0]$), the hit probabilities are large and pollution rates are very small, suggesting that the color–color diagram of $u-g$ versus $g-r$ can separate N-rich stars

[13] The color–color diagrams at other metallicity ranges could be found in Figure A2 in Appendix.

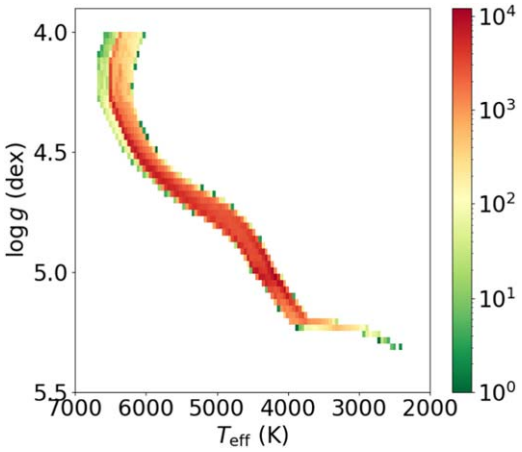

Figure 5. The Kiel diagram of selected dwarf stars, with color representing the number density.

from normal stars with a high efficiency. The hit probabilities for each metallicity bin are larger than that for the full metallicity bin—dividing the metallicity range can help us select more N-rich dwarf stars.

3.3. Identification of N-rich Stars with Slitless Spectrograph

A slitless spectrograph ($R \sim 200$) in the main survey module of the CSST covers several strong C, N, O related molecular features, and thus should be suitable for separating N-rich stars from normal stars (see Section 2). To evaluate the required signal-to-noise ratio (SNR) for observation, we synthesized spectra with $R \sim 200$ using ISPEC. Then Poisson noise was added to the synthetic spectra to simulate CSST observed spectra with SNR of 20/10.

We picked one star with stellar parameters around the median values of the giant star sample as representative. Two spectra following the chemical patterns of N-rich stars (green lines) and normal stars (blue lines) were generated, respectively (e.g., upper panel of Figure 7(a)). To clearly visualize the molecular features, we calculated the flux ratio between the two spectra aforementioned (e.g., lower panel of Figure 7(a)). To further estimate their significance level, we fitted Gaussian profiles (red lines) to the molecular bands in the flux ratio spectra. We used the maximum depth of the Gaussian function to represent the "signal" of a molecular band (labeled as "A"). Then the "noise" (σ) is calculated as the standard deviation of flux ratios from 450 to 500 nm. Finally, we define the ratio of "signal" to "noise" as the significance level of each feature. Three molecular features stand out clearly: NH3400, CN3839 and CN4142. Under an SNR of 20, the significance levels of NH3400, CN3839, and CN4142 are 39.1σ, 31.7σ, and 9.2σ, respectively, which are labeled in the bottom-left in the lower panel of Figure 7(a). Under an SNR of 10, the significance

Table 1
The Pollution Rate, Hit Probability, and Coefficients of Division Lines for Giant Stars without Photometric Error

[Fe/H] Bin	Pollution Rate	Hit Probability	a_0	a_1	a_2	a_3	a_4	a_5
$-1.2 <$ [Fe/H] < -1.0	1.57e–01	17.47%	−1.790	8.931	−6.535	1.112	1.653	−0.739
$-1.4 <$ [Fe/H] < -1.2	1.36e–02	24.76%	2.732	−18.027	55.059	−67.090	38.330	−8.424
$-1.6 <$ [Fe/H] < -1.4	1.51e–02	10.55%	3.937	−25.291	72.353	−87.648	50.343	−11.173
$-1.8 <$ [Fe/H] < -1.6	9.68e–03	15.14%	4.796	−30.073	81.638	−95.357	52.768	−11.272
$-1.8 <$ [Fe/H] < -1.0	3.95e–02	7.72%	−2.549	13.164	−16.203	12.090	−4.448	0.580

Note. $y = a_0 + a_1x + a_2x^2 + a_3x^3 + a_4x^4 + a_5x^5$, $x = g$–r, $y = u$–g.

Table 2
The Pollution Rate, Hit Probability, and Coefficients of Division Lines for Dwarf Stars without Photometric Error

[Fe/H] Bin	Pollution Rate	Hit Probability	a_0	a_1	a_2	a_3	a_4	a_5
$-1.2 <$ [Fe/H] < -1.0	7.82e–02	31.45%	3.750	−24.691	73.863	−92.609	53.678	−11.812
$-1.4 <$ [Fe/H] < -1.2	9.41e–02	29.47%	3.680	−24.571	73.921	−93.185	54.305	−12.012
$-1.6 <$ [Fe/H] < -1.4	8.35e–02	30.20%	3.659	−24.817	75.092	−95.292	55.907	−12.448
$-1.8 <$ [Fe/H] < -1.6	6.84e–02	35.62%	3.813	−26.336	79.847	−102.050	60.359	−13.549
$-1.8 <$ [Fe/H] < -1.0	5.44e–02	13.01%	3.750	−24.691	73.863	−92.609	53.678	−11.812

Note. $y = a_0 + a_1x + a_2x^2 + a_3x^3 + a_4x^4 + a_5x^5$, $x = g$–r, $y = u$–g.

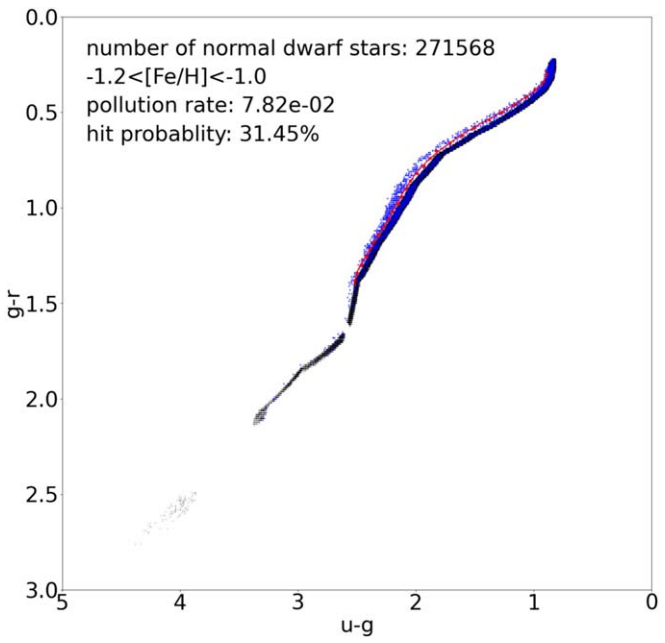

Figure 6. $u - g$ versus $g - r$ for N-rich dwarf stars (blue) and normal dwarf stars (black) at $-1.2 <$ [Fe/H] < -1.0. Symbol meanings are the same as in Figure 4. The red curve ranges from $g - r = 0.28$ mag to 1.40 mag.

levels of these molecular bands are 27.0σ, 24.8σ, and 8.8σ, respectively. As the SNR decreases, the significance levels of the molecular bands decrease. The significance levels are larger than 5σ under an SNR of 10, suggesting that a spectrum with an SNR of 10 is sufficient for separating N-rich giant stars from normal giant stars.

We did the same for a representative star from the dwarf star sample (Figure 8). Compared to the giant stars, only the NH3400 feature is significantly different between an N-rich star and a normal star. The significance level of NH3400 is 53.6σ under an SNR of 20 and 25.2σ under an SNR of 10, both of which are larger than 5σ. This suggests that a spectrum with an SNR of 10 is sufficient for separating N-rich dwarf stars from normal dwarf stars.

Given that N-rich stars can be identified in slitless spectra with a given SNR, there is concern about how to identify them from tens of millions of spectra. There are multiple methods to carry out such investigation: 1. one can calculate the spectral indices related to N feature lines, and select those with extreme values. This method is carefully outlined in Tang et al. (2019, 2020); 2. one can find out the N-rich stars with strong N-related features by applying the outlier detection algorithm on slitless spectra with similar stellar parameters; etc.

4. Discussion

There are two practical issues on photometric identification of N-rich stars. The first one is how accurately can we measure the metallicity from the CSST main survey photometry? Utilizing training with artificial intelligence, Haibo Yuan (private communication) suggested that the retrieved metallicity accuracy is $\sim$ 0.1 dex for FGK solar-scaled abundance stars, which is less than the metallicity bin width of 0.2 dex used in photometric identification. However, metallicity is

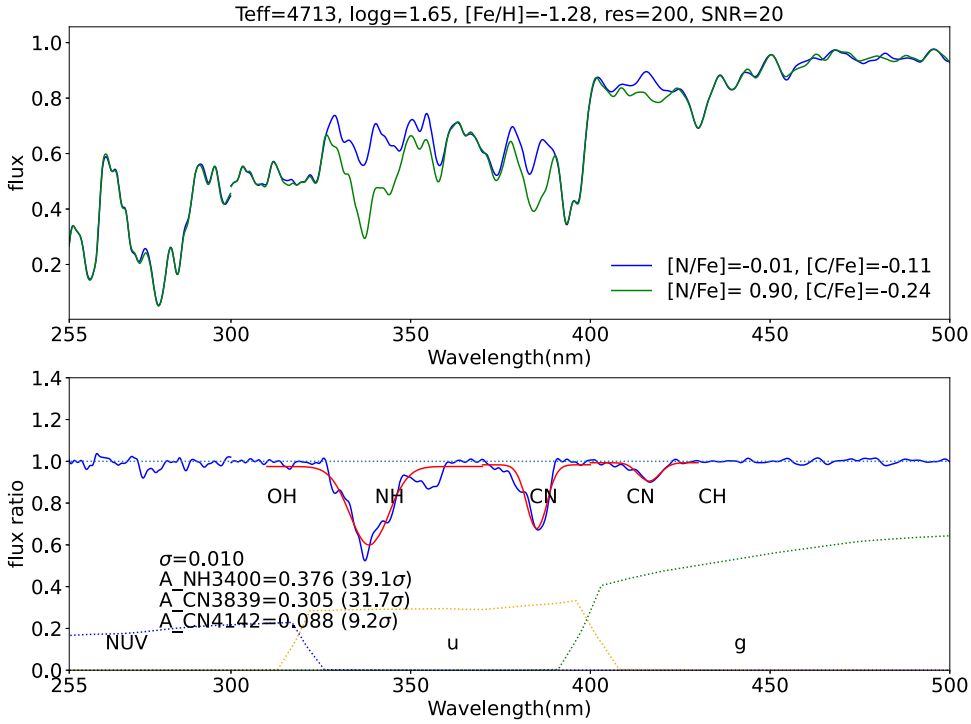

(a) SNR = 20

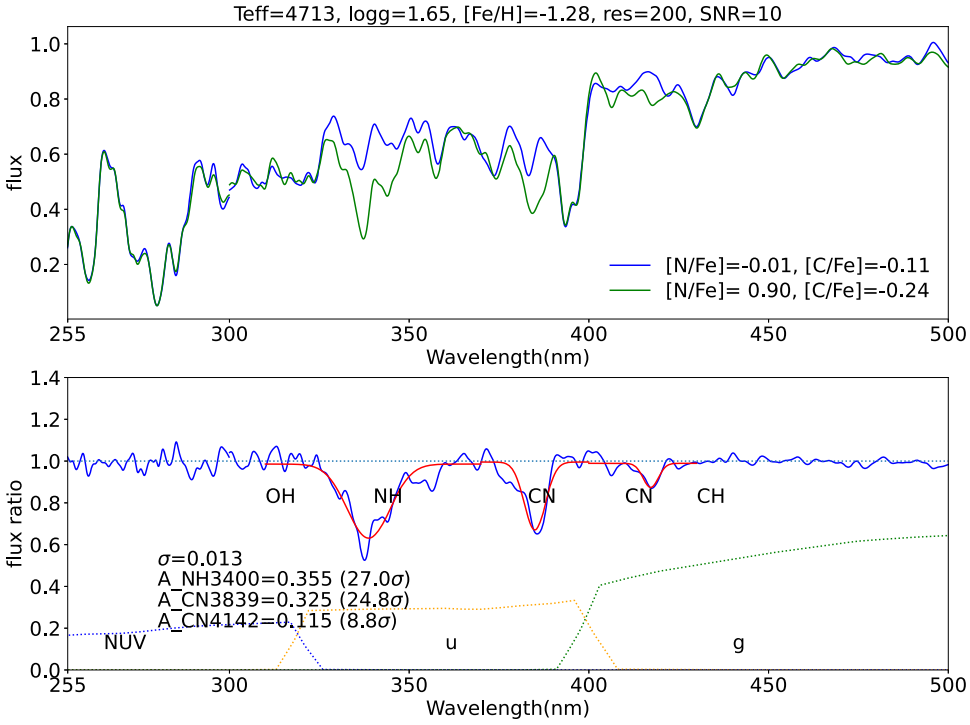

(b) SNR = 10

Figure 7. Synthetic spectra with SNR of 20 (a) and 10 (b) for a representative giant star. Symbols have the same meanings as in Figure 1. Additionally, we calculated the significance level of strong molecular features, and listed their values in the bottom-left. See the text for more details.

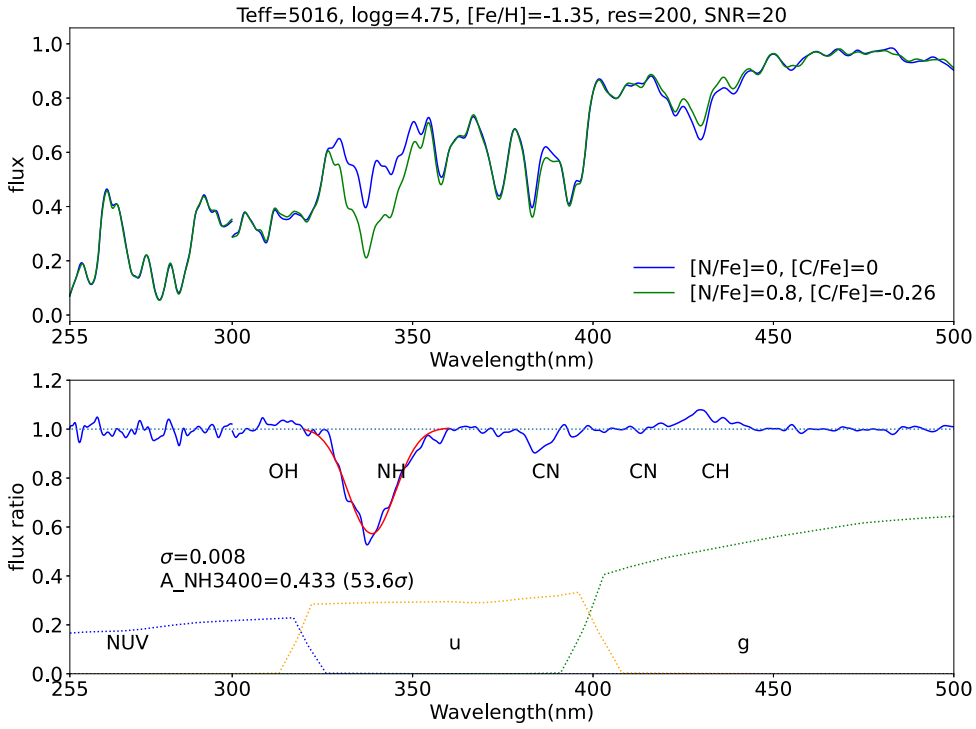

(a) SNR = 20

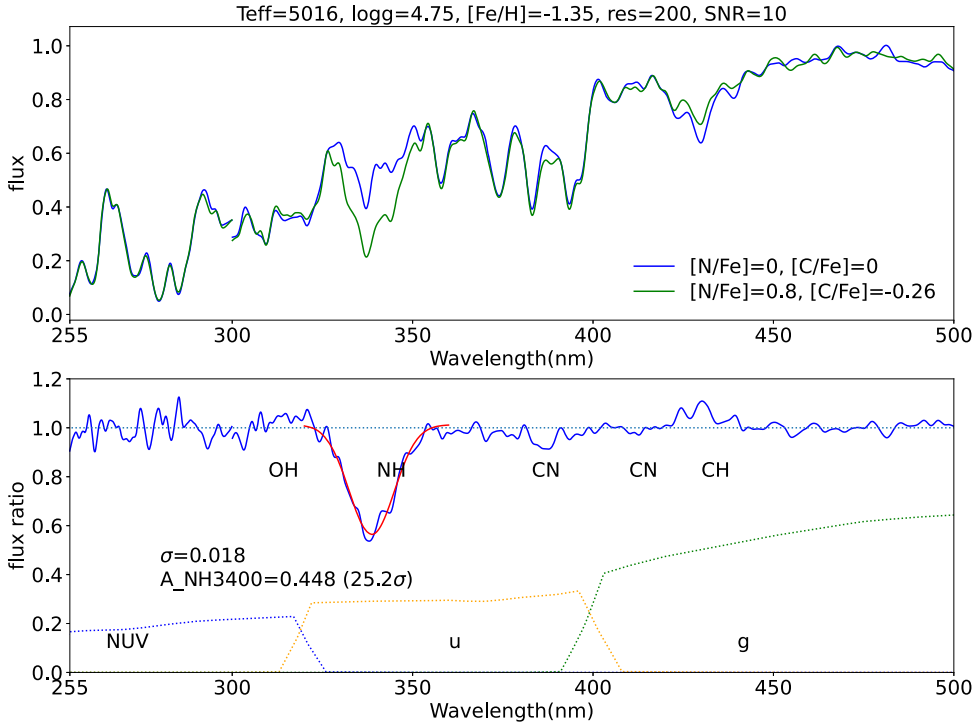

(b) SNR = 10

Figure 8. Synthetic spectra with SNR of 20 (a) and 10 (b) for a representative dwarf star. See the text for more details.

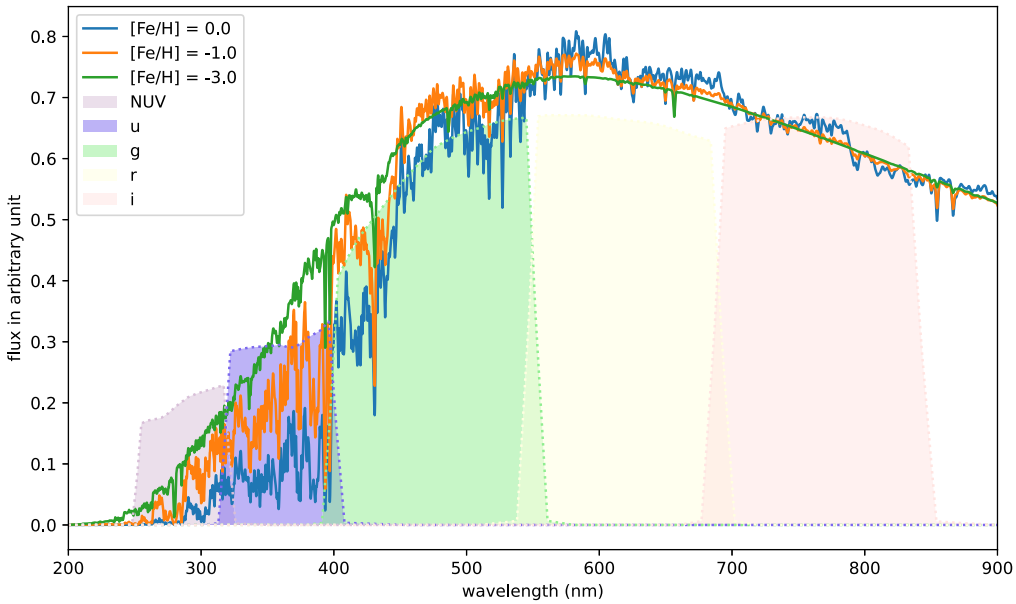

Figure 9. Three synthetic spectra for three red giant stars with the same effective temperature and surface gravity but different metallicity. The effective temperature is 4700 K, and the surface gravity is 1.5. The blue, orange, and green lines represent metallicity equal to 0.0, −1.0, and −3.0, respectively. The spectra come from the PHOENIX synthetic library (Husser et al. 2013). Three spectra are normalized using the flux ranging from 700 to 750 nm. The shadow areas with different colors represent the throughput of CSST filters.

derived based on its strong impact on *u*-band magnitudes, which is also affected by N abundances. Thus, there is concern about the degeneracy between deriving metallicity and N abundances based on *u*-band magnitudes. To break this degeneracy, filters that are sensitive to either metallicity or N abundances could be helpful. Theoretically, the *NUV* band should be more sensitive to metallicity compared to the *u* band, because of the numerous metal lines in the former band. To verify this, we retrieve spectra from the PHOENIX synthetic library[14] (Husser et al. 2013). Figure 9 shows the flux differences in *NUV* and *u* band filters for three red giant stars with different metallicities. The *NUV*-band magnitude is clearly sensitive to [Fe/H], but not to [N/H], given that there are no strong N-related features in this band (see Figures 7 and 8). Therefore, the aforementioned degeneracy can be broken with *NUV*-band magnitude or related colors. However, the relatively poor studies in oscillator strength of absorption features in this band prevent us from further investigation. Besides, it is also beyond the scope of this paper. Hopefully, the upcoming CSST photometric and spectroscopic observations in the *NUV* band can provide calibration to the theoretical spectra. Since most metal-poor halo stars are alpha-enhanced, we further discuss if *u*-band photometry is strongly affected by [alpha/Fe]. Following the procedure above, we retrieved two spectra from the PHOENIX synthetic library with [alpha/Fe] = 0.2 and 0.4 at $T_{\rm eff} = 4700$ K, $\log g = 1.5$, [Fe/H] = −1.0. We find that the magnitude difference in the *u*-band is negligible (∼0.005 mag). Therefore, alpha-enhancement does not affect the [N/H] determination.

The second one is the impact of photometric error. We added photometric errors of *u, g, r* bands for all the stars in our catalog according to Qu et al. (2023). After adding photometric errors, the efficiency of identifying N-rich stars from normal stars drops significantly due to the large photometric errors of fainter stars. To avoid large photometric errors that blur the boundaries, we limited our sample to brighter stars. In the end, we find $g = 18.5$ mag achieves a good balance between maximizing sample size and minimizing pollution rate (Tables 3 and 4). In these two tables, we found reasonable hit probabilities and pollution rates, suggesting that the method is valid for bright stars ($g < 18.5$ mag). The color–color diagrams of $u - g$ versus $g - r$ are depicted in Figures 10 and 11 between the metallicity bin of [−1.2, −1.0] at $g < 18.5$ mag. Though 18.5 mag may seem bright in photometric surveys, it is in fact fainter than any currently identified N-rich field stars, as spectroscopic observations are required.

5. Conclusion

GCs are one of the oldest stellar systems in our MW, which witnessed the formation and evolution of the latter. During their co-evolution, GC stars can escape to the field, and retracing these stars is crucial for depicting the details of MW evolution. The N-rich nature of chemically enhanced

[14] https://phoenix.astro.physik.uni-goettingen.de/

Table 3
The Pollution Rate, Hit Probability, and Coefficients of Division Lines for Giant Stars with Photometric Error

[Fe/H] Bin	Pollution Rate	Hit Probability	a_0	a_1	a_2	a_3	a_4	a_5
$-1.2 <$ [Fe/H] < -1.0	2.90e–01	34.44%	−2.011	11.076	−13.419	10.607	−4.251	0.626
$-1.4 <$ [Fe/H] < -1.2	2.78e–01	34.79%	5.176	−31.625	84.673	−98.796	55.028	−11.881
$-1.6 <$ [Fe/H] < -1.4	2.89e–01	18.01%	5.992	−36.954	97.916	−114.788	64.398	−14.028
$-1.8 <$ [Fe/H] < -1.6	2.75e–01	13.16%	6.545	−39.944	103.637	−119.564	65.977	−14.130
$-1.8 <$ [Fe/H] < -1.0	2.99e–01	17.17%	−1.361	7.587	−6.270	3.527	−0.848	−0.011

Note. $y = a_0 + a_1x + a_2x^2 + a_3x^3 + a_4x^4 + a_5x^5$, $x = g$–r, $y = u$–g.

Table 4
The Pollution Rate, Hit Probability, and Coefficients of Division Lines for Dwarf Stars with Photometric Error

[Fe/H] Bin	Pollution Rate	Hit Probability	a_0	a_1	a_2	a_3	a_4	a_5
$-1.2 <$ [Fe/H] < -1.0	2.92e–01	16.91%	3.495	−22.774	68.750	−86.034	49.632	−10.871
$-1.4 <$ [Fe/H] < -1.2	2.14e–01	27.50%	3.745	−24.945	75.017	−94.771	55.338	−12.251
$-1.8 <$ [Fe/H] < -1.6	2.50e–01	30.00%	−1.513	27.416	−128.157	285.045	−287.176	107.230
$-1.8 <$ [Fe/H] < -1.0	3.01e–01	17.83%	3.408	−22.078	66.615	−83.273	48.060	−10.544

Note. (1) We do not list relative information at the metallicity bin of [−1.6, −1.4], because the pollution rate is high when the quantile is 100% at $g < 18.0$ mag. The range of application of the division line is $0.28 < g - r < 1.15$ at the metallicity bin of [−1.4, −1.2] and $0.28 < g - r < 0.9$ at the metallicity bin of [−1.8, −1.6], while for other metallicity bins, the range is $0.28 < g - r < 1.4$.
(2) $y = a_0 + a_1x + a_2x^2 + a_3x^3 + a_4x^4 + a_5x^5$, $x = g$–r, $y = u$–g.

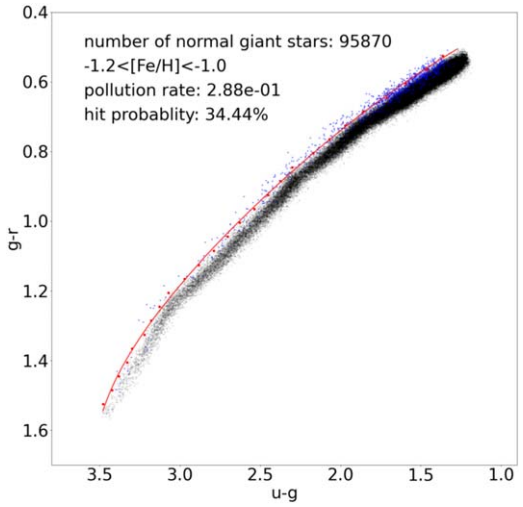

Figure 10. $u - g$ vs. $g - r$ for giant stars with photometric error at $g <$ 18.5 mag and $-1.2 <$ [Fe/H] < -1.0. Symbol meanings are the same as in Figure 4.

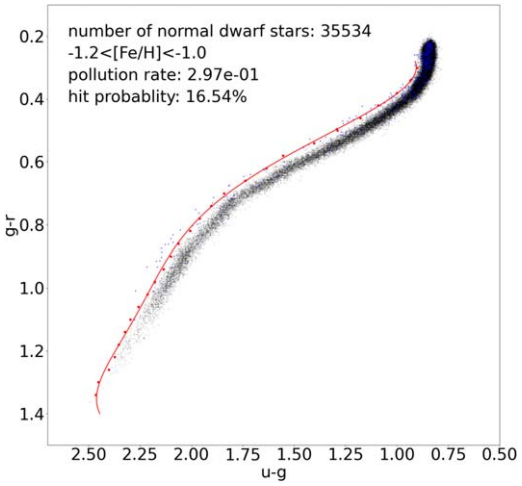

Figure 11. $u - g$ vs. $g - r$ for dwarf stars with photometric error at $g <$ 19.0 mag and $-1.2 <$ [Fe/H] < -1.0. Symbol meanings are the same as in Figure 6.

populations in GCs offers a bright future for identifying GC escapees with *UV* photometry and spectroscopy, e.g., CSST. Based on the mock photometric catalog of MW halo stars, we evaluated the efficiency of identifying N-rich stars for giants and dwarfs, separately. We used ISPEC to generate spectra with various chemical patterns, and added Poisson noise to mimic observed spectra with SNR of 10 and 20. We demonstrated that slitless spectra ($R \sim 200$) with an SNR of 10 are sufficient to identify N-related molecular features with significance greater than 5σ, and thus are able to separate N-rich stars from normal stars. In parallel, we generated spectra with different chemical patterns and convolved them with CSST main survey filters to simulate their magnitude differences. We found that the color–color diagram of $u - g$ versus $g - r$ is a potential way to identify N-rich stars, since u band covers the strong NH and CN molecular features.

Based on our mock catalog, we will identify a much larger number of N-rich stars than before. This large sample with an unprecedented size will be a comprehensive sample to test different MW formation scenarios, e.g., results from *N*-body simulations. For example, Gieles & Gnedin (2023) evaluated the mass loss rates of GCs with stellar-mass black holes, where they found an agreement for density profiles of N-rich (field) stars between models and observations (see their Figure 12), confirming that these stars originated from GCs. In the near future, the largest sample of N-rich (field) stars identified using CSST photometry will reveal their spatial distribution, velocity distribution and even chemical abundances at a statistically significant level. Further combination with state-of-the-art *N*-body simulations will be promising to address many details during the MW evolution.

Acknowledgments

J.Z., B.T., C.L., and L.W. gratefully acknowledge support from the China Manned Space Project Nos. CMS-CSST-2021-B03, CMS-CSST-2021-A08, and _____, the National Natural Science Foundation of China under grant No. 12233013, 12073090, and the Natural Science Foundation of Guangdong Province under grant No. 2022A1515010732. J.G.F.-T. gratefully acknowledges the grant support provided by Proyecto Fondecyt Iniciación No. 11220340, and also from ANID Concurso de Fomento a la Vinculación Internacional para Instituciones de Investigación Regionales (Modalidad corta duración) Proyecto No. FOVI210020, and from the Joint Committee ESO-Government of Chile 2021 (ORP 023/2021), and from Becas Santander Movilidad Internacional Profesores 2022, Banco Santander Chile. L.W. thanks the support from the National Natural Science Foundation of China through grant 21BAA00619, the one-hundred-talent project of Sun Yat-sen University, the Fundamental Research Funds for the Central Universities, Sun Yat-sen University (22hytd09).

Appendix
Additional Figures

We display the color–color diagrams of $u-g$ versus $g-r$ at the metallicity bin of [-1.8, -1.0], [-1.4, -1.2], [-1.6, -1.4] and [-1.8, -1.6] as below. Figure A1 is for giants and Figure A2 is for dwarfs.

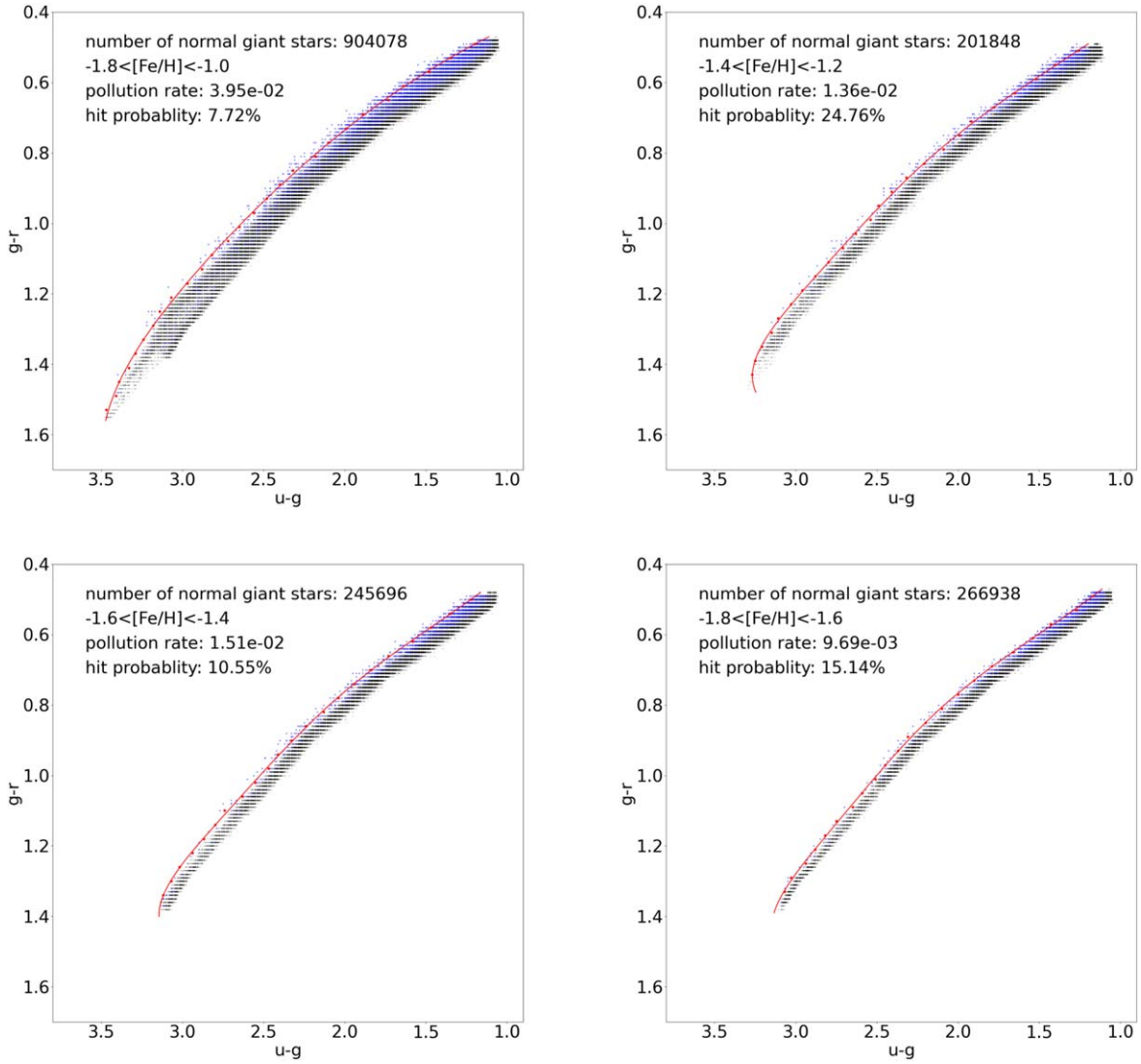

Figure A1. $u - g$ versus $g - r$ for N-rich giant stars (blue) and normal giant stars (black) at different metallicity ranges. Symbol meanings are the same as in Figure 4.

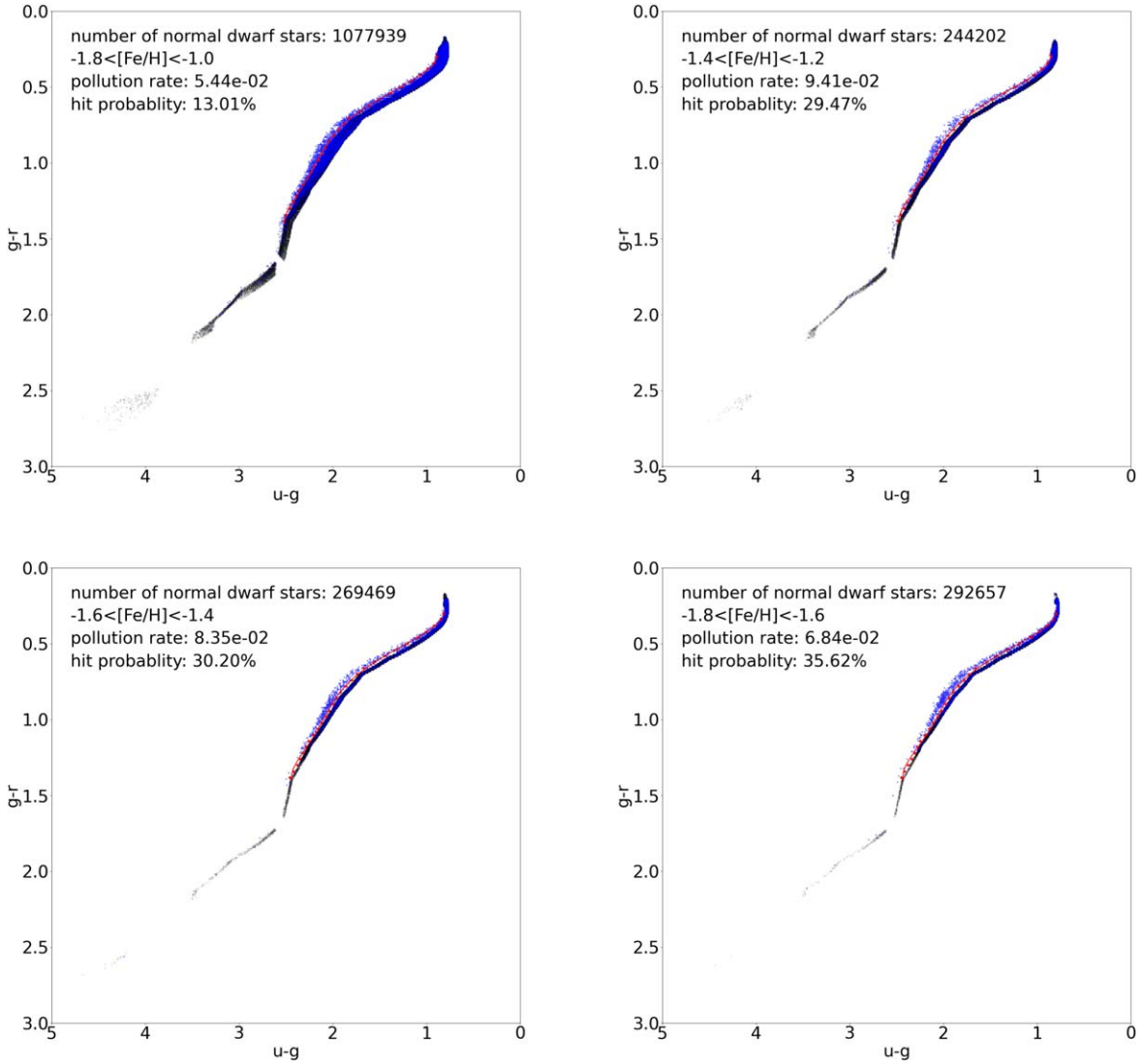

Figure A2. $u - g$ versus $g - r$ for N-rich dwarf stars (blue) and normal giant stars (black) at different metallicity ranges. Symbol meanings are the same as in Figure 6.

ORCID iDs

Jiajun Zhang https://orcid.org/0000-0003-1352-7226
Hao Tian https://orcid.org/0000-0003-3347-7596
Yang Huang https://orcid.org/0000-0003-3250-2876

References

Asplund, M., Grevesse, N., Sauval, A. J., & Scott, P. 2009, ARA&A, 47, 481
Blanco-Cuaresma, S. 2019, MNRAS, 486, 2075
Blanco-Cuaresma, S., Soubiran, C., Heiter, U., & Jofré, P. 2014, A&A, 569, A111
Bullock, J. S., & Boylan-Kolchin, M. 2017, ARA&A, 55, 343
Fernández-Trincado, J. G., Beers, T. C., Minniti, D., et al. 2020, ApJL, 903, L17
Fernández-Trincado, J. G., Beers, T. C., Minniti, D., et al. 2021, A&A, 648, A70
Gieles, M., & Gnedin, O. Y. 2023, MNRAS, 522, 5340
Gratton, R. G., Carretta, E., & Bragaglia, A. 2012, A&Ar, 20, 50
Gray, R. O., 1999 SPECTRUM: A stellar spectral synthesis program, Astrophysics Source Code Library, ascl:9910.002
Gustafsson, B., Edvardsson, B., Eriksson, K., et al. 2008, A&A, 486, 951
Husser, T. O., Wende-von Berg, S., Dreizler, S., et al. 2013, A&A, 553, A6
Li, C., Zheng, Z., Li, X., et al. 2022, RAA, 22, 095004
Majewski, S. R., Schiavon, R. P., Frinchaboy, P. M., et al. 2017, AJ, 154, 94
Martell, S. L., & Grebel, E. K. 2010, A&A, 519, A14
Martell, S. L., Shetrone, M. D., Lucatello, S., et al. 2016, ApJ, 825, 146
Martell, S. L., Smolinski, J. P., Beers, T. C., & Grebel, E. K. 2011, A&A, 534, A136
Masseron, T., García-Hernández, D. A., Mészáros, S., et al. 2019, A&A, 622, A191
Mészáros, S., Masseron, T., García-Hernández, D. A., et al. 2020, MNRAS, 492, 1641
Nataf, D. M., Wyse, R. F. G., Schiavon, R. P., et al. 2019, AJ, 158, 14
Pang, X.-Y., Olczak, C., Guo, D.-F., Spurzem, R., & Kotulla, R. 2016, RAA, 16, 37
Qu, H., Yuan, Z., Doliva-Dolinsky, A., et al. 2023, MNRAS, 523, 876
Schiavon, R. P., Johnson, J. A., Frinchaboy, P. M., et al. 2017a, MNRAS, 466, 1010
Schiavon, R. P., Zamora, O., Carrera, R., et al. 2017b, MNRAS, 465, 501
Sharma, S., Bland-Hawthorn, J., Johnston, K. V., & Binney, J. 2011, ApJ, 730, 3
Shetrone, M., Tayar, J., Johnson, J. A., et al. 2019, ApJ, 872, 137
Tang, B., Fernández-Trincado, J. G., Liu, C., et al. 2020, ApJ, 891, 28
Tang, B., Liu, C., Fernández-Trincado, J. G., et al. 2019, ApJ, 871, 58
Weatherford, N. C., Kıroğlu, F., Fragione, G., et al. 2023, ApJ, 946, 104
Yanny, B., Rockosi, C., Newberg, H. J., et al. 2009, AJ, 137, 4377
Yu, J., Tang, B., Fernández-Trincado, J. G., et al. 2021, ApJ, 913, 23
Zhan, H. 2021, ChSBu, 66, 9
Zhao, G., Zhao, Y.-H., Chu, Y.-Q., Jing, Y.-P., & Deng, L.-C. 2012, RAA, 12, 723